EISENSTEIN, M. (1979). *Acta Cryst.* B**35**, 2614-2655.
EISENSTEIN, M. & HIRSHFELD, F. L. (1983). *Acta Cryst.* B**39**, 61-75.
HARADA, J. (1988). *Aust. J. Phys.* **41**, 351-357.
HIRSHFELD, F. L. & HOPE, H. (1980). *Acta Cryst.* B**36**, 406-415.
HÖCHE, H. R., SCHULZ, H., WEBER, H.-P., BELZNER, A., WOLF, A. & WULF, R. (1986). *Acta Cryst.* A**42**, 106-110.
HOPE, H. & OTTERSEN, T. (1978). *Acta Cryst.* B**34**, 3623-3626.
HUANG, K. (1947). *Proc. R. Soc. (London) Ser. A.* **190**, 102-117.
KHEIKER, D. M. (1969). *Acta Cryst.* A**25**, 82-88.
LADELL, J. & SPIELBERG, N. (1966). *Acta Cryst.* **21**, 103-122.
MATHIESON, A. MCL. (1982). *Acta Cryst.* A**38**, 378-387.
MATHIESON, A. MCL. (1983). *J. Appl. Cryst.* **16**, 572-573.
MATHIESON, A. MCL. (1984*a*). *Acta Cryst.* A**40**, 355-363.
MATHIESON, A. MCL. (1984*b*). *Aust. J. Phys.* **37**, 55-61.
MATHIESON, A. MCL. (1988). *Acta Cryst.* A**44**, 239-243.
MATHIESON, A. MCL. & STEVENSON, A. W. (1985). *Acta Cryst.* A**41**, 290-296.
OHBA, S., SATO, Y., SAITO, Y., OHSHIMA, K.-I. & HARADA, J. (1983). *Acta Cryst.* B**39**, 49-53.
OTTERSEN, T., ALMHOF, J. & CARLE, J. (1982). *Acta Chem. Scand. Ser. A*, **36**, 63-68.
OTTERSEN, T., ALMHOF, J. & HOPE, H. (1980). *Acta Cryst.* B**36**, 1147-1154.
OTTERSEN, T. & HOPE, H. (1979). *Acta Cryst.* B**35**, 373-378.
WERNER, S. A. (1971). *Acta Cryst.* A**27**, 665-669.
WERNER, S. A. (1972). *Acta Cryst.* A**28**, 143-151.
YOUNG, R. A. (1969). *Acta Cryst.* A**25**, 55-66.

Acta Cryst. (1989). A**45**, 620-628

High-Voltage Electron Diffraction from Bacteriorhodopsin (Purple Membrane) is Measurably Dynamical

BY R. M. GLAESER

Biophysics Department and the Donner Laboratory, Lawrence Berkeley Laboratory, University of California, Berkeley, CA 94720, *USA*

AND T. A. CESKA

NRC Biotechnology Research Institute, 6100 *Royalmount Ave, Montreal, Quebec, Canada H4P 2R2*

(*Received* 7 *November* 1988; *accepted* 7 *April* 1989)

Abstract

Electron diffraction patterns of 45 Å thick two-dimensional crystalline arrays of a cell membrane protein, bacteriorhodopsin, have been recorded at two electron voltages, namely 20 and 120 kV. Significant intensity differences are observed for Friedel mates at 20 kV, but deviations from Friedel symmetry are quite small at 120 kV. It does not seem likely that the measured Friedel differences can be accounted for by complex atomic structure factors, by curvature of the Ewald sphere, or by effects that might occur as a result of inelastic scattering (absorption). It is therefore concluded that dynamical diffraction within the single molecular layer of these crystals is responsible for the observed Friedel differences. The results are useful in estimating the maximum specimen thickness for which the kinematic approximation may be safely used in electron crystallography of biological macromolecules at the usual electron voltage of 100 kV, or even at higher voltages. The results show that the Friedel differences are independent of resolution and this opens up the possibility that dynamical effects occurring at lower voltages might be used to phase higher-voltage kinematic diffraction intensities.

Introduction

Bacteriorhodopsin is a protein of molecular weight 27 000 which naturally forms well ordered monolayer crystals within the cell membrane of *Halobacterium halobium.* These crystalline patches, known as purple membrane, are readily isolated from the bacteria as small membrane fragments only 45 Å thick (Blaurock, 1975; Henderson, 1975) and typically 0·3 μm^2 in area. Single-crystal X-ray diffraction patterns cannot be measured from these specimens because of the small size of the purple membrane fragments. Electron diffraction and high-resolution electron microscopy therefore represent the method of choice for a crystallographic structure analysis of the constituent protein, bacteriorhodopsin. Progress in this structure analysis, which includes a three-dimensional density map at 6 Å and a two-dimensional projection at 3·5 Å resolution, has been reviewed by Baldwin, Ceska, Glaeser & Henderson (1987).

The use of electron diffraction and high-resolution image data to produce Coulomb potential density maps has so far assumed that the electron-specimen interaction can be described to a satisfactory degree of accuracy by the weak-phase-object (WPO) approximation (Hoppe, 1970; Erickson, 1974; Amos, Henderson & Unwin, 1982). The WPO approximation is a simplified version of the single-scattering kinematic approximation, in which the Ewald sphere is approximated as a plane (Glaeser, 1985). Other factors that are ignored in the WPO approximation, but which can affect the experimental data, include

0108-7673/89/090620-09$03.00

spatial modulation of the amplitude of the electron wave due to inelastic scattering, Fresnel diffraction within the finite thickness of the specimen, and multiple elastic scattering within the finite thickness of the specimen. Multiple elastic scattering invalidates the simple Fourier transform relationship between the Coulomb potential and the diffracted wave amplitude, a relationship which makes the kinematic (and the WPO) approximation so powerful for crystallographic structure determinations. Multiple elastic scattering and Fresnel propagation within the specimen are accounted for by the Cowley-Moodie formulation of the dynamical diffraction theory (Cowley & Moodie, 1957; Jap & Glaeser, 1978). Unfortunately, the mathematical description of dynamical diffraction only permits the calculation of diffraction patterns or electron microscope images for a known or a model structure. The dynamical theory does not yet provide a general inverse operation by which images or diffraction intensities can be used for the direct determination of unknown structures. There is some progress in dynamical theory, however, which has resulted in a method for the determination of structure-factor phases from rather special dynamical effects (Shen & Colella, 1987).

In structural studies performed so far with bacteriorhodopsin, which have used electrons at voltages up to 120 kV, there has been no previous indication of measurable dynamical effects in the data. The absence of significant dynamical effects at these voltages, for organic materials as thin as purple membrane, is consistent with theoretical simulations on related materials, using the Cowley-Moodie formulation of dynamical diffraction theory (Jap & Glaeser, 1980; Ho, Jap & Glaeser, 1988).

It is recognized, however, that the situation with complex structures like purple membrane must represent an unusually favorable case, since the interaction of 100 kV electrons with much simpler organic structures, or with materials composed of atoms with higher atomic number, will certainly be strongly dynamical at a thickness of 50 Å. As an example, the (1, 1) and (2, 0) diffraction spots of monolayer crystals of *n*-paraffin ($C_{36}H_{74}$) have experimentally measured wave amplitudes that are approximately 0·14 times the amplitude of the unscattered beam at 100 kV (Henderson & Glaser, 1985). In the case of high-atomic-number compounds, the classic study of Glauber & Schomaker (1953) demonstrated that significant dynamical effects occur even within single molecules of UF_6, at 40 kV.

The large unit-cell dimension of purple membrane (hexagonal, $a = 62{\cdot}45$ Å) means that many diffracted beams will be simultaneously excited, a situation that is further ensured by the fact that the Fourier transform of a monolayer crystalline specimen is a continuous function along the parallel set of reciprocal-lattice lines. Although even the strongest diffraction spots of purple membrane have a wave amplitude that is no more than 0·005 times the unscattered wave amplitude at 100 kV (Unwin & Henderson, 1975), the large number of beams that can interact dynamically, through multiple scattering, creates a situation in which significant deviations might occur from a simple Fourier transform relationship between the scattering object and the diffracted wave.

We now report the results of diffraction experiments that have been performed with purple membrane, using both 20 and 120 kV electrons. These experiments have been performed in part to define better the conditions under which the single scattering approximation may be safely applied in the interpretation of electron crystallographic data for biological macromolecules, and in part to determine whether measurable dynamical effects can be observed, which might ultimately prove to be useful in phasing the higher-voltage kinematic data.

We have observed rather large departures from Friedel symmetry in 20 kV electron diffraction patterns, like the anomalous differences seen when diffraction patterns are obtained with X-rays at a wavelength close to the absorption edge of one or more atoms in a structure. Some significant Friedel differences are also observable even at 120 kV, but they are smaller than those seen at 20 kV. Extrapolation of the results of our measurements using purple membrane suggests that the kinematic approximation will result in a generally acceptable degree of error for specimen thicknesses of at least 100 Å at 120 kV, and for specimen thicknesses of at least 200 Å at 400 kV.

Methods

Glucose-embedded specimens of fused purple membranes were placed on carbon-coated grids and electron diffraction patterns were recorded under low-dose conditions (Baldwin & Henderson, 1984). Grids were mounted in a Philips cold holder at room temperature and inserted into the microscope; after prescanning a couple of grid holes, the stage was cooled to −120 °C (153 K). All diffraction patterns were recorded at low temperature. Film densitometry and extraction of background-subtracted intensities were performed as described by Baldwin & Henderson (1984) with the exception that the signed difference between the Friedel-related reflections was preserved. Scaling, temperature factor and tilt angle were determined for each film by refining against a three-dimensional 120 kV purple membrane electron diffraction data set (Ceska & Henderson, unpublished). The diffraction patterns used were from untwinned membranes. The maximum specimen tilt was found to be less than 2·5°.

Additional programs were written to compute various quantities from scaled data. Diffraction

Table 1. *Intensities, percent Friedel differences and summary for* (1, 2) *reflections at* 120 kV *and* 20 kV

The Friedel differences are expressed as a percentage of the average intensity of the corresponding Friedel pair of reflections, there being three such symmetry-related measurements on each film. The standard error of the mean has been calculated as the root mean square difference divided by the square root of the number of observations.

Film number	120 kV intensity	120 kV % Friedel difference	Film number	20 kV intensity	20 kV % Friedel difference
5258	1818	−15	5269	1779	−38
	1747	−28		1960	−52
	1582	−28		1817	−32
5265	1929	−16	5270	1728	−41
	1705	−24		1787	−40
	1696	−15		1779	−49
5503	1362	24	5581	1747	−39
	1553	−9		1890	−30
	1481	−23		1815	−43
5505	1735	−27	5585	1776	−47
	1677	−34		1611	−55
	1764	−41		1591	−48
Average (absolute value)		21·8			42·9
Standard error of the mean		4·3			2·1

patterns were compared with a consistent hand, and diffraction intensities from separate films were re-indexed to achieve equivalent indexing of (h, k) *versus* $(-h, -k)$ reflections. This last step could always be done without ambiguity because of the large Friedel differences for the (1, 2) reflections. Observations from four films at each voltage were included in the calculations. After merging the data together, Friedel differences were expressed as a percentage of the average intensity of the two reflections comprising a Friedel pair. The average (percent) Friedel difference and the standard error of the mean were then calculated for the complete set of observations, which could include as many as 12 Friedel pairs for each Miller index. Table 1 shows a representative example of the data used in these calculations, corre-

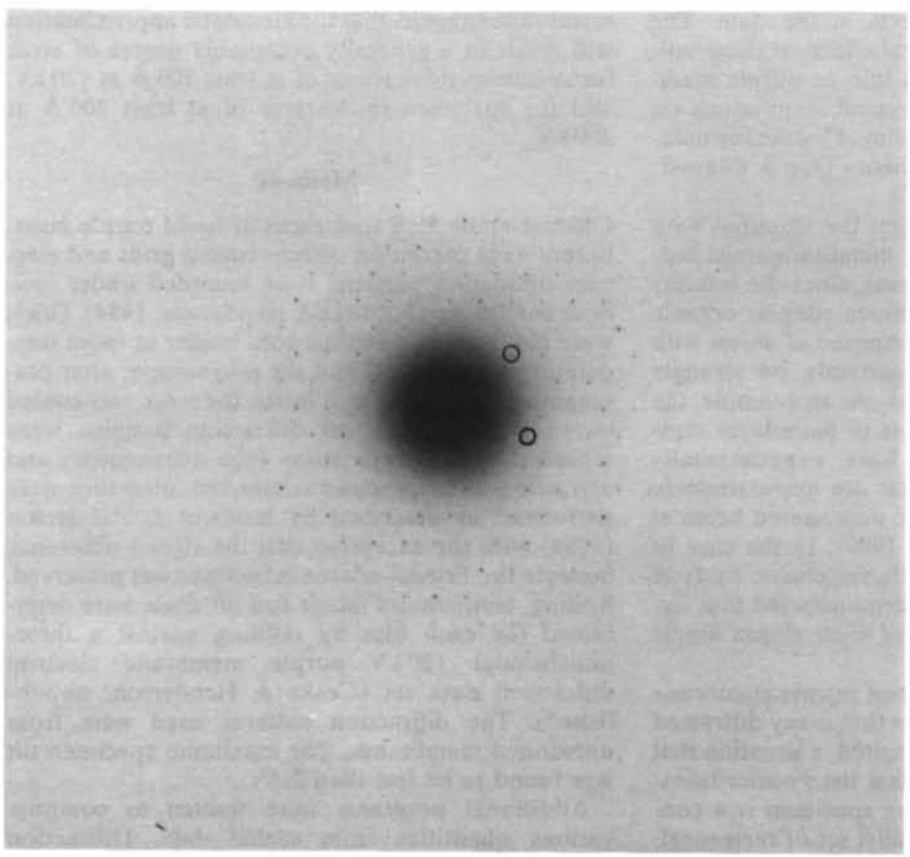

Fig. 1. Electron diffraction pattern (20 kV) from a glucose-embedded purple membrane sample. The deviation from Friedel symmetry is just detectable by examining the low-resolution reflections around the central blackening. The (1, 2) reflection has been circled.

sponding to the Friedel differences observed for the (1, 2) reflections at 120 kV and at 20 kV. Data from the (3, 3) reflection were excluded from the analysis because they showed excessive variability, which we believe to be due to extreme sensitivity to tilt, and data from the (1, 0) and (1, 1) were too close to the central spot to be used.

The absolute ratio of diffraction intensities at 20 and at 120 kV was obtained by first measuring $I(g)/I(0)$, the ratio of the diffraction intensity for each spot to the intensity of the unscattered beam, following the technique described by Henderson & Glaeser (1985). As before, the diffraction intensities were scaled and corrected for the estimated temperature factor. The central beam intensity determined the overall scale factor between the two data sets. The average value of $I(g)/I(0)$ was determined from three films at each voltage, and the ratio of the two average values was used to calculate the absolute ratio between each voltage, $I_{20}(g)/I_{120}(g)$.

Results

Electron diffraction patterns recorded at 20 kV show detectable intensity differences between Friedel pairs, a few of which are even recognizable by visual inspection of the diffraction pattern. A representative example of the sort of pattern that has been used in this work is shown in Fig. 1, and careful inspection will reveal a slight failure of Friedel symmetry for the (1, 2) family of diffraction spots. The excellent threefold symmetry of the diffraction intensities, particularly of the tilt-sensitive family of (4, 2) reflections, shows that the incident beam was very nearly perpendicular to the plane of the specimen.

Quantitative measurements, however, clearly show that there are significant intensity differences between Friedel pairs for many of the reflections. As shown in Table 2, the mean Friedel difference for the (1, 2) reflection is about 43% at 20 kV, which is much greater than the standard error of the mean, which is only 2·1%. Even at 120 kV the measured Friedel differences for the (1, 2) type reflections is approximately 22%. When data to 7 Å are examined, the average Friedel differences for all reflections is 16% at 20 kV, and 6% at 120 kV.

An overall summary is also presented in Table 2 of the magnitude of the systematic and random errors that are embedded in the present measurements. The column labeled $(\Delta I/\langle I\rangle)_{3\text{-fold}}$ presents the r.m.s. difference in intensity of individual members of symmetry-related triplets of diffraction spots, relative to their mean intensity. In addition to random intensity fluctuations (counting statistics) and errors in densitometry, the threefold intensity differences also reflect the intensity changes to be expected from small amounts of specimen tilt. For some reflections small differences in tilt angle result in large changes in intensity. This is especially true for the (3, 3) reflection. The standard error of the mean in the percent Friedel difference is included in the column labeled $(\Delta I/\langle I\rangle)_{\text{Friedel}}$. Although small amounts of specimen tilt introduce a certain degree of systematic error in the Friedel differences, since somewhat non-equivalent data are being compared at not-quite-threefold-related positions in reciprocal space, it is nevertheless reasonable to see that the Friedel differences for all reflections are considerably higher for the low-voltage data compared with the high-voltage data, and that the errors on each data set are about the same.

Table 2. *Comparison of Friedel intensity differences with the intensity differences arising from random error or from curvature of the Ewald sphere*

	$(\Delta I/\langle I\rangle)_{\text{Friedel}}$ (%)	$(\Delta I/\langle I\rangle)_{3\text{-fold}}$ (%)	$(\Delta I/\langle I\rangle)_{\text{curvature}}$ (%)
(1, 2)/20 kV	42·9 ± 2·1	4·2	0·3
(1, 2)/120 kV	21·8 ± 4·3	5·8	0·1
7 Å/20 kV	16·4 ± 3·3	16	4·1
7 Å/120 kV	6·41 ± 3·8	19	1·6

The finite curvature of the Ewald sphere introduces yet another systematic error in that the measurements of nominally Friedel-equivalent diffraction spots are, in fact, measurements at slightly non-equivalent positions in reciprocal space. Curvature of the Ewald sphere results (in the kinematic case) in sampling both the (h, k) reciprocal-lattice rod and the $(-h, -k)$ reciprocal-lattice rod at a height

$$z^* = 1/\lambda - [(1/\lambda)^2 - (1/d)^2]^{1/2}$$

where λ = electron wavelength, and d = Bragg spacing of the $hk0$ reflection.

When $d = 7$ Å and $\lambda = 0{\cdot}0859$ Å (20 kV), then $z^* = 0{\cdot}00088$ Å^{-1}, which is much smaller than the reciprocal of the specimen thickness ($1/45$ Å $= 0{\cdot}022$ Å^{-1}). Thus, intensity measurements at reciprocal-lattice points (h, k, z^*) and $(-h, -k, z^*)$ should not be much different from those at the true Friedel-related points (h, k, z^*) and $(-h, -k, -z^*)$. This qualitative argument notwithstanding, the availability of measured three-dimensional data at 120 kV (Ceska & Henderson, unpublished) makes it possible to estimate the actual intensity difference that should occur due only to curvature of the Ewald sphere. As shown in the third column of Table 2, this intensity difference at 20 kV is only 0·3% for the (1, 2) reflections, and it is only 4·1% for the full data set out to 7 Å. At progressively higher resolution, curvature of the Ewald sphere would naturally result in large differences at 20 kV. Extension of the present data analysis to high resolution therefore requires the proper indexing of measured intensities by z^* and the collection of separate three-dimensional intensity curves for (h, k) and $(-h, -k)$ reciprocal-lattice lines. It is clear, however, that curvature of the Ewald sphere

does not play an important role in accounting for the measured Friedel differences for purple membrane, as long as the analysis is limited to 7 Å.

Looking at the measurements in detail, we find that there is no significant correlation between the magnitude of the Friedel difference and the resolution (*i.e.* spatial frequency); see Figs. 2(*a*) and (*b*). On the other hand, the percent Friedel differences are rather strongly correlated with the intensity of the reflection, the percent difference being generally much larger for weak reflections than for strong reflections, as is shown in Fig. 3(*a*). In all, of the 32 unique reflections, 24 show an averge Friedel difference at least three times the standard error of the mean at 20 kV, while five show an average Friedel difference at least three times the standard error of the mean at 120 kV. The percent Friedel differences at 120 kV (Fig. 2*a*) are much smaller than those at 20 kV (Fig. 2*b*), but even so the size of the Friedel difference at 120 kV is strongly correlated to the size of the Friedel difference at 20 kV, as shown in Fig. 3(*b*).

Apart from the anomalous Friedel differences just discussed, another indication of failure of the kinematic approximation is found when the absolute intensities of equivalent diffraction spots are compared at low (20 kV) and high (120 kV) voltages. The ratio of the relativistic electron velocity at 120 kV to that at 20 kV is 2·158. If the diffraction intensities were kinematic in both cases, then the absolute intensities at 20 kV should all be equal to the square of this ratio, or 4·65, times the intensities at 120 kV. The measured 20 kV intensities are generally much greater than predicted by kinematic theory, relative to the 120 kV intensities. While the ratio shows no systematic correlation with the intensity of the reflection (Fig. 4*a*), there is a definite tendency for the lower-resolution reflections to have a larger ratio than the higher-resolution reflections (Fig. 4*b*).

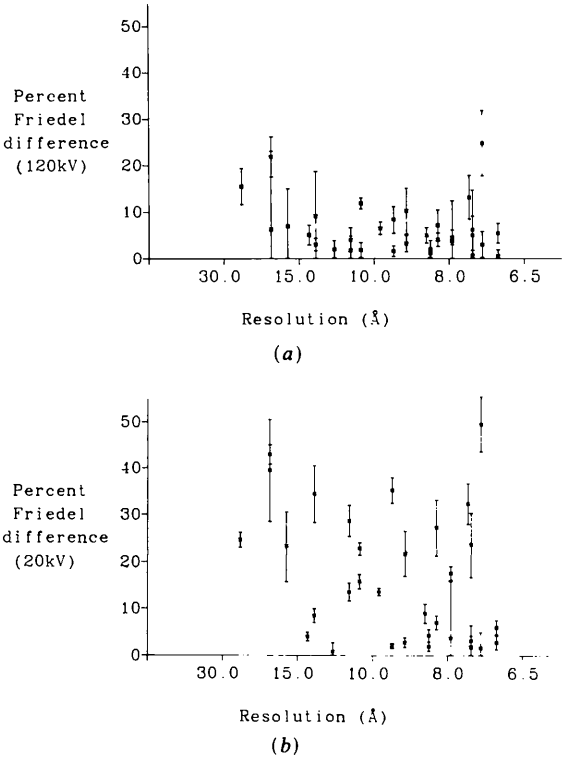

Fig. 2. Friedel intensity differences. (*a*) The percent Friedel differences from diffraction patterns taken at 120 kV. (*b*) The percent Friedel differences from diffraction patterns taken at 20 kV. The plots show that there is no correlation with resolution.

Theoretical considerations

Considering structures with relatively high atomic number, Hoerni (1956*a*) has shown that the use of complex atomic scattering factors in a pseudo-kinematic approximation results in accurate interpretations of gas-phase 40 kV electron scattering from

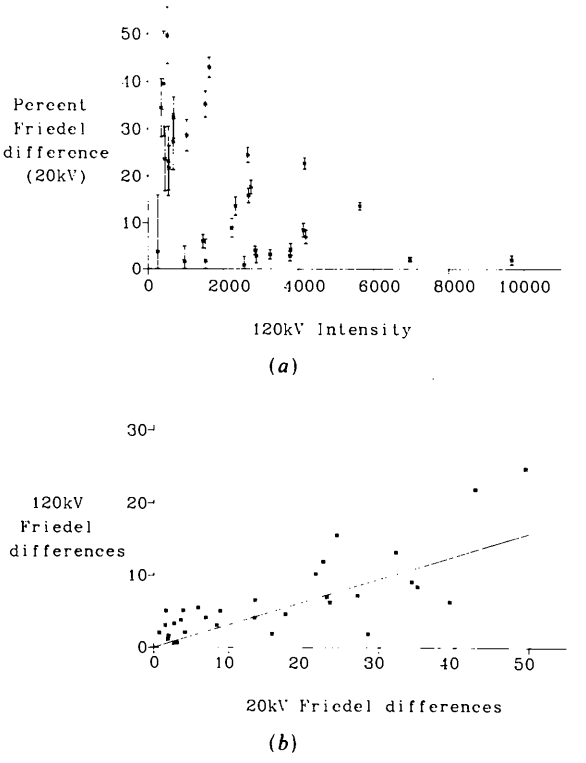

Fig. 3. Systematic trends in the Friedel differences. (*a*) The percent Friedel differences at 20 kV plotted against 120 kV diffraction intensity values shows the tendency of the lower-intensity reflections to have the larger percent Friedel differences. (*b*) The magnitude of observed Friedel differences at 120 kV for a particular (*h*, *k*) plotted as a function of the corresponding magnitude at 20 kV for the same reflection, showing the high degree of correlation. The straight line is a least-squares best fit to the data. Smaller Friedel differences are expected at 120 kV than at 20 kV if they are, in fact, the result of dynamical diffraction, since the strength of the scattering interaction decreases with increasing electron velocity.

small molecules. This approximation represents, however, only a marginal improvement over the kinematic approximation in describing electron diffraction from thin crystals (Hoerni, 1956*b*). The pseudo-kinematic approximation will result in failure of Friedel symmetry provided that there are at least two types of atoms present in the structure, each of which has a distinctly different ratio of real and imaginary parts for its respective atomic scattering factors. For high-voltage electrons the atomic scattering factors are inherently complex, a fact that can be attributed to higher-order terms in the Born series. Failure of the first Born approximation for hydrogen atoms is relatively small, while the effects for carbon, nitrogen and oxygen are quite comparable to one another. If we write the atomic scattering factors for carbon and hydrogen, respectively, as

$$f_{C,N,O} = |f_{C,N,O}| \exp(i\eta_{C,N,O})$$

$$f_H = |f_H| \exp(i\eta_H),$$

the molecular structure factors at a spatial frequency

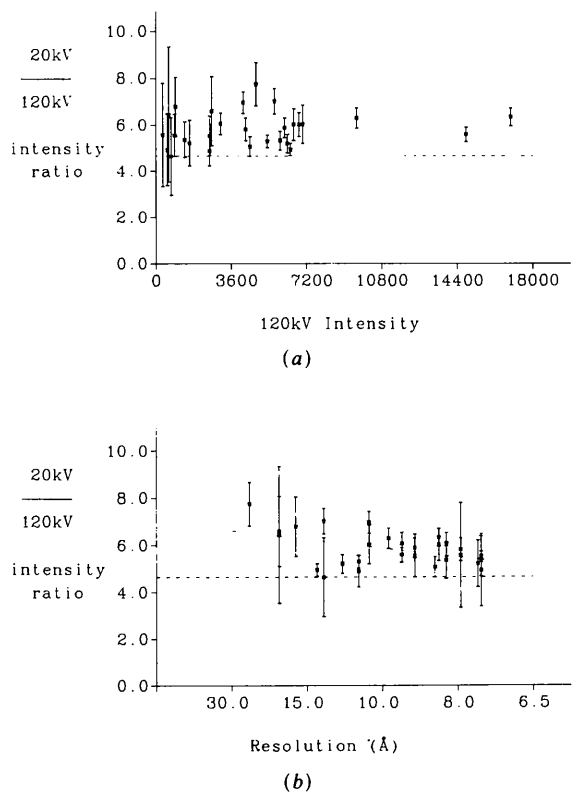

Fig. 4. The ratio of absolute intensities, 20 kV to 120 kV. The kinematic ratio of intensities should be 4·65 (see text). (*a*) Absolute intensity ratio plotted against 120 kV intensity. The ratio is not correlated with reflection intensity. (*b*) Absolute intensity ratio plotted as a function of resolution. The ratio tends to get higher at low resolution.

g and its Friedel mate at $-g$ are

$$F(g) = |F_{C,N,O}| \exp(i\eta_{C,N,O}) \exp(i\varphi_{C,N,O}) + |F_H| \exp(i\eta_H) \exp(i\varphi_H)$$

$$F(-g) = |F_{C,N,O}| \exp(i\eta_{C,N,O}) \exp(-i\varphi_{C,N,O}) + |F_H| \exp(i\eta_H) \exp(-i\varphi_H).$$

The ratio of the Friedel difference to the average intensity of a Friedel pair can be expressed as

$$\frac{\Delta I}{\langle I \rangle} = \frac{4x \sin(\Delta\varphi) \sin(\Delta\eta)}{1 + x^2 + 2x \cos(\Delta\varphi) \cos(\Delta\eta)}$$

where $x = |F_{C,N,O}|/|F_H|$; $\Delta\varphi = \varphi_{C,N,O} - \varphi_H$, and φ is the phase of the crystal structure factor, *i.e.* the kinematic diffracted wave; and $\Delta\eta = \eta_{C,N,O} - \eta_H$, and η is the phase of the atomic scattering factor.

The relative intensity difference has a maximum value of 2·0 when $x = 1{\cdot}0$ and when $\Delta\varphi = \pi \pm \Delta\eta$. Thus it is mathematically possible for the pseudo-kinetic effect to produce Friedel differences even larger than the differences observed experimentally. It is unlikely, however, that our measurements can really be accounted for by pseudo-kinematic effects, when one takes into consideration the calculated values of atomic scattering factors, f, the phases, η, and the known chemical structures of proteins. For example, the calculated values of f and η which have been published in *International Tables for X-ray Crystallography* (Bonham & Schäfer, 1974) and elsewhere (Raith, 1968) indicate that $f_{C,H,O}/f_H$ is about 5 and $\Delta\eta$ is about 0·07 at 20 kV. Varying only $\Delta\varphi$, we find that the maximum for the function written above is

$$\max\left(\frac{\Delta I}{\langle I \rangle}\right) = 2\left[1 + \frac{(1-x^2)^2}{4x^2 \sin^2(\Delta\eta)}\right]^{-1/2}.$$

Since the expectation value for x is about 5, the expected Friedel differences are only about 0·1%. If it is argued that x might still have values close to 1 for some reflections, then it would be necessary for $\Delta\varphi$ to have values larger than 120° in order to produce Friedel differences as large as 25%. Such large values of $\Delta\varphi$ cannot occur in real protein structures because the spatial distribution of H atoms is necessarily very similar to the spatial distribution of C, N and O atoms; thus the phases φ_H and $\varphi_{C,N,O}$ must also be quite similar.

The amount of inelastic scattering will vary from point to point in a sample of inhomogeneous chemical composition and structure. Inelastic scattering will therefore impose a spatially varying amplitude modulation on the wave function of the transmitted (elastic) electrons. Inclusion of the effects of inelastic scattering therefore causes the specimen to behave as a mixed phase and amplitude object, with a consequent failure of Friedel's law. While the quantitative theory of amplitude modulation due to inelastic scattering

is not well developed, a few relevant points can still be discussed.

The amount of inelastic scattering can be expected to be greater in regions of the specimen that have increased mass thickness, as is also the case for the phase modulation, but the delocalized nature of most of the inelastic scattering events (Isaacson, Langmore & Rose, 1974) will tend to smooth out the amplitude modulation relative to the corresponding phase modulation. Because of the delocalization effect, it is unlikely that inelastic scattering would produce significant amplitude modulations of the transmitted wave at resolutions much higher than about 10 Å. No significant reduction is seen, however, when the percent Friedel difference is plotted as a function of resolution.

The effects of inelastic scattering can be represented phenomenologically in the WPO approximation by an imaginary part of the Coulomb potential, resulting in a transmitted wave function

$$T(x) \simeq 1 - i(2\pi/hv)\,V_1(x) - (2\pi/hv)\,V_2(x),$$

where $V_1(x)$ is the real part of the potential and $V_2(x)$ is the imaginary part of the potential, h is Planck's constant and v is the electron velocity. The transmitted intensity for the unscattered and elastically scattered electrons is then

$$I_T(x) \simeq 1 - (4\pi/hv)\,V_2(x).$$

From these two equations it is evident that the amplitude grating term in $T(x)$, for a weak object, is of the same order of magnitude as half the inelastic scattering cross section, which in turn is comparable to the elastic scattering cross section in the case of carbon, nitrogen and oxygen. The phase grating term, on the other hand, is of order of magnitude of the elastic scattering amplitude, not the cross section. For a weak object, then, $V_2 \ll V_1$, and inelastic scattering is unable to explain large departures from Friedel symmetry in the diffraction intensities.

Finally, the ratio of elastic to inelastic scattering cross section does not change very much with the incident electron voltage. Thus, the ratio of V_2 to $(V_1)^2$, and hence the ratio of V_2 to V_1, must be almost constant from 20 to 120 kV. If inelastic scattering (*i.e.* absorption) were the cause of the observed Friedel differences, then the Friedel difference would have to be the same at 20 and at 120 kV. The fact that this is not the case clearly rules out absorption as the principal cause of the observed Friedel differences.

Discussion

Dynamical electron diffraction causes a small but measurable failure of Friedel's law in the electron diffraction intensities recorded for purple membrane at 120 kV, and a substantially larger failure at 20 kV. The measured differences between Friedel mates are frequently too large to be attributed to random intensity fluctuations (counting statistics) or errors in densitometry. Curvature of the Ewald sphere is expected to introduce a systematic error, or difference, between nominal Friedel mates, but it is shown here that this effect is smaller than the random errors in our measurements. Theoretical considerations show that the Friedel differences cannot be due to the amplitude modulations that must result from inelastic scattering, and therefore the Friedel differences reflect a true failure of the kinematic or weak-phase-object approximation. Theoretical considerations also show that the measured Friedel differences are unlikely to be accounted for as the anomalous differences which must occur when corrections to the Born approximation are used for atomic scattering factors. The measured Friedel differences there seem to be due to dynamical coupling of diffracted beams, *i.e.* multiple scattering within the 45 Å thick specimen.

The observation of significant intensity differences between Friedel pairs in purple membrane diffraction patterns at 20 kV has important implications for the rapidly developing field of electron crystallography of biological macromolecules. To begin with, these experimental data provide an independent check on existing theoretical estimates of the validity of the kinematic approximation. Secondly, a quantitative measurement of these differences makes it possible to estimate the probable accuracy of the kinematic approximation at higher electron voltages and at greater specimen thicknesses. Finally, the existence of measurable intensity differences between Friedel pairs opens up the possibility that dynamical diffraction effects might be used to phase diffraction data, a field which is nevertheless still in its early stages of development, even for X-ray diffraction patterns (Colella, 1974; Post, 1977; Shen & Colella, 1987).

The measured Friedel differences at 20 and 120 kV show that dynamical diffraction is somewhat more important in electron diffraction of biological macromolecules than one might have previously expected, based upon the theoretical calculations for a protein molecule, cytochrome b_5 (Ho, Jap & Glaeser, 1988). The theoretical calculations were used to evaluate the importance of dynamical effects by calculating the crystallographic residual, R, which is the r.m.s. difference in amplitudes for the dynamical and WPO approximations, respectively. Based upon that criterion, which is of course different from our present criterion of Friedel differences, it seems that r.m.s. intensity differences of 10 to 20% should not occur, at 100 kV, for a macromolecular specimen less than 200 Å in thickness. The theoretical calculations are only an approximation to the real circumstances, however. For example, the calculations assume that the WPO approximation can be used to describe wave propagation through individual 30 Å thick layers of the cytochrome b_5 crystal, corresponding to the c-axis

repeat. The calculations do not include hydrogen atoms or bound solvent, nor do they include the effects of complex-valued atomic scattering factors. Finally, it should be mentioned that wave propagation through bacteriorhodopsin may be somewhat more dynamical than through cytochrome b_5 because of the presence of long α-helices in bacteriorhodopsin, which are oriented perpendicular to the plane of the membrane, resulting in strong reinforcement of the projected Coulomb potential of one atom on top of another in the peptide backbone. Taking all factors into consideration, we find that the conclusion that measurable dynamical effects occur in the electron diffraction intensities of purple membrane, even at 120 kV, is not in marked disagreement with theoretical expectations. The present experiments do indicate, however, that the previous theoretical calculations have underestimated the magnitude of dynamical effects that can occur in electron crystallography of biological molecules.

The magnitude of the observed dynamical effects must be put into perspective in the context of crystallographic structure analysis. The fact that departures from the WPO approximation become measurable does not suddenly imply that large errors in the structure analysis will occur or that the resulting density maps will be unreliable. The dynamical effects measured for purple membrane at 120 kV are generally quite small, and they occur preferentially in the weaker reflections (which contribute relatively little to the final density). The magnitude of the Friedel differences at 20 kV is perhaps large enough, however, that one would have to be cautious about interpreting the data by the kinematic (or WPO) approximation.

The present experimental data and previous theoretical calculations (Ho, Jap & Glaeser, 1988) can be used to estimate the sample thickness at which dynamical effects are likely to become as marked at 100 kV, or higher voltages, as they are for purple membrane at 20 kV. The interaction constant for elastic scattering scales, of course, inversely with electron velocity, which is $0{\cdot}27c$ (c is the velocity of light) at 20 kV, $0{\cdot}55c$ at 100 kV, and $0{\cdot}83c$ at 400 kV. To a first approximation one would then expect to see the same degree of dynamical interaction, in the limit of suitably small dynamical effects, at roughly twice the sample thickness when going from 20 to 100 kV and then again from 100 kV to the relativistic limit. This rough estimate does indeed correspond to the thickness and voltage dependence of dynamical effects that were found in the theoretical calculations for cytochrome b_5. On this basis one might then project generally that dynamical effects for macromolecules will be no worse at 100 kV than those observed for purple membrane at 20 kV, provided that the specimen thickness is less than $\sim$100 Å, while specimens up to 200 Å in thickness might be used at voltages close to the relativistic limit, *e.g.* 400 kV. There is no black-and-white cutoff for these estimates, however, and each investigator will have to decide how much of a departure from the kinematic or WPO regime can be tolerated in the particular crystallographic structure analysis that may be under consideration.

The use of weak dynamical effects to phase the kinematic structure factors is a matter that warrants further consideration, in view of the now-established fact that there are measurable intensity differences which may be attributable to multiple elastic scattering. A simplified approach would be to interpret intensity differences between the high-voltage (supposedly kinematic) limit and some chosen lower voltage as being solely due to double scattering at the lower voltage. The intensity differences would then be expressible as simultaneous transcendental equations in the unknown phases, with cross products of the (known) kinematic amplitudes as coefficients. Iterative solution of these equations would then be required; the availability of accurate lower-resolution phases from images would clearly be an advantage in starting the iterative solution. In order to test this approach it would be important to collect a data set of $(h, k, 0)$ diffraction intensities at two voltages, in which individual measurements are indexed first according to their (h, k, z^*) values, including both the effects of specimen tilt and curvature of the Ewald sphere. Smooth curves could then be fit to the measurements to produce the desired $(h, k, 0)$ values at a resolution that is limited only by the crystalline order of the specimen. Experiments to measure such data at low voltage are now in progress.

We would like to thank Dr Paul Sigler for discussions in the initial stages of this work, and Dr Dieter Typke for valuable contributions to our discussion of the pseudo-kinematic approximation. TAC gratefully acknowledges fellowship support from NSERC (Canada). This work has been partially supported by National Institutes of Health grant GM 36884.

References

AMOS, L. A., HENDERSON, R. & UNWIN, P. N. T. (1982). *Prog. Biophys. Mol. Biol.* **39**, 183-231.

BALDWIN, J. M., CESKA, T. A., GLAESER, R. M. & HENDERSON, R. (1987). In *Crystallography in Molecular Biology*, edited by D. MORAS, J. DRENTH, B. STRANDBERG, D. SUCK & K. WILSON, pp. 101-105. New York: Plenum.

BALDWIN, J. M. & HENDERSON, R. (1984). *Ultramicroscopy*, **14**, 319-336.

BLAUROCK, A. E. (1975). *J. Mol. Biol.* **93**, 139-158.

BONHAM, R. A. & SCHÄFER, L. (1974). In *International Tables for X-ray Crystallography*, Vol. IV, pp. 176-269. Birmingham: Kynoch Press. (Present distributor Kluwer Academic Publishers, Dordrecht.)

COLELLA, R. (1974). *Acta Cryst.* A**30**, 413-423.

COWLEY, J. M. & MOODIE, A. F. (1957). *Acta Cryst.* **10**, 609-619.

ERICKSON, H. P. (1974). *Adv. Opt. Electron Microsc.* **5**, 163-199.

GLAESER, R. M. (1985). *Annu. Rev. Phys. Chem.* **36**, 243-275.

GLAUBER, R. & SCHOMAKER, V. (1953). *Phys. Rev.* **89**, 667-671.
HENDERSON, R. (1975). *J. Mol. Biol.* **93**, 123-138.
HENDERSON, R. & GLAESER, R. M. (1985). *Ultramicroscopy*, **16**, 139-150.
HO, M.-H., JAP, B. K. & GLAESER, R. M. (1988). *Acta Cryst.* A**44**, 878-884.
HOERNI, J. A. (1956*a*). *Phys. Rev.* **102**, 1530-1533.
HOERNI, J. A. (1956*b*). *Phys. Rev.* **102**, 1534-1542.
HOPPE, W. (1970). *Acta Cryst.* A**26**, 414-426.
ISAACSON, M., LANGMORE, J. P. & ROSE, H. (1974). *Optik (Stuttgart)*, **41**, 92-96.
JAP, B. K. & GLAESER, R. M. (1978). *Acta Cryst.* A**34**, 94-102.
JAP, B. K. & GLAESER, R. M. (1980). *Acta Cryst.* A**36**, 57-67.
POST, B. (1977). *Phys. Rev. Lett.* **39**, 760-763.
RAITH, H. (1968). *Acta Cryst.* A**24**, 85-93.
SHEN, W. & COLELLA, R. (1987). *Nature (London)*, **329**, 232-233.
UNWIN, P. N. T. & HENDERSON, R. (1975). *J. Mol. Biol.* **94**, 425-440.

Acta Cryst. (1989). A**45**, 628-635

Structural Comparisons Using Restrained Inhomogeneous Transformations

BY SIMON K. KEARSLEY

Merck Sharp & Dohme Research Laboratories, PO Box 2000, *Rahway, NJ* 07065, *USA*

(*Received* 5 *May* 1988; *accepted* 10 *April* 1989)

Abstract

Comparisons between structures with similar atomic skeletons are made by mathematically deforming one over the other using inhomogeneous transformations. Removal of shallow bending and twisting distortions between the structures reveals local differences that are masked by comparisons using homogeneous transformations. Inhomogenous deformations are restrained to prevent unrealistic changes in local atomic bonding geometry by the addition of penalty functions similar in form to the potentials used in empirical molecular mechanics calculations.

1. Introduction

On many occasions chemists dealing with atomic structures need to measure the similarity for arrangements of corresponding atoms between two structures. For instance, a common requirement of crystallographers is to determine the similarity between two or more molecules that may pack within the asymmetric unit; also, they may wish to decide whether there exists any pseudo spatial symmetry between such molecules. Often comparisons of experimental structures to ones predicted by theoretical models are used to detect anomalies that may exist in either one. For molecular mechanics calculations, especially those of macromolecules, one is never guaranteed to find the same equilibrium structure. If several subtly different structures are generated then methods to compare and contrast them are essential.

The most common way to make a comparison between two structures is to superimpose them such that the sum of the squared distances between corresponding atoms is a minimum. This method maintains rigid structural skeletons. The use of the root mean square (r.m.s.) deviation of distance between these atoms as the measure of similarity between structures is ubiquitous since it is easy to appreciate. Slightly more sophisticated comparisons also measure relative amounts of compression or expansion between structures. These types of comparisons, termed orthogonal and homogeneous transformations respectively, often make similar conformations look radically different or conceal local differences between structures. Fig. 1 shows this in a schematic manner. Comparison method *A* merely superimposes without structural distortion, and the deviations in the region of the glitch are of the same magnitude as other regions; in atomic structures such localized differences between the arrangement of atoms are not easily seen.

Inhomogeneous transformations allow various types of bending and twisting distortions to occur. Low-order inhomogeneous transformations are defined as ones that give moderately shallow deformations that apply uniformly over the entire structure. The use of these is not in vogue since the prospect of performing and interpreting the resulting structural distortions is forbidding. But more significantly the number of degrees of freedom, even for low-order deformations, increases rapidly (a 60-parameter fit

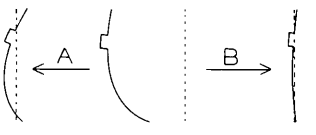

Fig. 1. Schematic illustration showing the effects of orthogonal (*A*) and inhomogeneous (*B*) comparison transformations.

0108-7673/89/090628-08$03.00